1   **Insights into the loss factors of phytoplankton blooms: The role of cell mortality in**

2   **the decline of two inshore *Alexandrium* blooms**

3

4

5   Chang Jae Choi[1,3], Michael L. Brosnahan[2], Taylor R Sehein[2], Donald M. Anderson[2] and

6   Deana L. Erdner[*,1]

7

8

9   [*]Corresponding author: Deana L. Erdner, The University of Texas at Austin, Marine

10   Science Institute, Port Aransas, TX 78373 USA phone: +1 361 749 6719; fax: +1 361

11   749 6777; e-mail: derdner@utexas.edu

12

13   [1]The University of Texas at Austin, Marine Science Institute, Port Aransas, TX 78373

14   USA

15   [2]Biology Department, Woods Hole Oceanographic Institution, Woods Hole, MA 02543

16   USA

17   [3]Current address: Monterey Bay Aquarium Research Institute, 7700 Sandholdt Road,

18   Moss Landing, CA 95039 USA

19

24   **Abstract**

25   While considerable effort has been devoted to understanding the factors regulating the

26   development of phytoplankton blooms, the mechanisms leading to bloom decline and

27   termination have received less attention. Grazing and sedimentation have been invoked as

28   the main routes for the loss of phytoplankton biomass, and more recently, viral lysis,

29   parasitism and programmed cell death (PCD) have been recognized as additional removal

30   factors. Despite the importance of bloom declines to phytoplankton dynamics, the

31   incidence and significance of various loss factors in regulating phytoplankton populations

32   have not been widely characterized in natural blooms. To understand mechanisms

33   controlling bloom decline, we studied two independent, inshore blooms of *Alexandrium*

34   *fundyense*, paying special attention to cell mortality as a loss pathway. We observed

35   increases in the number of dead cells with PCD features after the peak of both blooms,

36   demonstrating a role for cell mortality in their terminations. In both blooms, sexual cyst

37   formation appears to have been the dominant process leading to bloom termination, as

38   both blooms were dominated by small-sized gamete cells near their peaks. Cell death and

39   parasitism became more significant as sources of cell loss several days after the onset of

40   bloom decline. Our findings show two distinct phases of bloom decline, characterized by

41   sexual fusion as the initial dominant cell removal processes followed by elimination of

42   remaining cells by cell death and parasitism.

43 **Introduction**

44 Phytoplankton dynamics are driven by imbalances between growth and loss processes

45 that in turn are controlled by a combination of physical (e.g. temperature, light,

46 turbulence), chemical (e.g. nutrients, oxygen) and biological (e.g. life cycle, grazing)

47 factors (Cloern 1996). Blooms occur when growth processes are dominant over losses,

48 then decline when loss processes intensify relative to growth. The mechanisms

49 underlying loss processes are diverse and poorly constrained. Traditionally, grazing by

50 heterotrophic zooplankton and sinking into the deep ocean have been considered the main

51 loss factors for phytoplankton (Calbet and Landry 2004). However, natural populations

52 and laboratory cultures often collapse abruptly due to massive cell lysis events, indicating

53 that different processes must be contributing to phytoplankton mortality (Berges and

54 Falkowski 1998; Vardi et al. 1999; Berges and Choi 2014). Virus-induced cell lysis is

55 increasingly recognized as an important alternative loss factor, with a large number of

56 viruses found in aquatic ecosystems (Brussaard 2004). There is evidence that chronic

57 parasitic infections can be an important cause of phytoplankton population crashes as

58 well (Chambouvet et al. 2008).

59 Another loss mechanism that has received increased attention in recent years is

60 autocatalyzed cell mortality, such as programmed cell death (PCD). PCD is different

61 from other pathways of cell death because it is an active process that is initiated by the

62 cell itself and tightly controlled by gene expression and protein synthesis inside of the

63 cells (Bidle and Falkowski 2004). Accumulating evidence suggests that PCD occurs in

64 phytoplankton under diverse environmental stresses, such as light and nutrient

65 deprivation, high temperature and salinity, UV exposure and oxidative stress in both

66   laboratory and natural populations (Segovia et al. 2003; Bidle and Bender 2008; Jauzein

67   and Erdner 2013). Thus, PCD is another potentially important pathway for phytoplankton

68   mortality that can explain abrupt bloom termination in some natural and laboratory

69   systems. Indeed, PCD as an agent for bloom termination has been described in naturally-

70   occurring blooms of the dinoflagellate *Peridinium gatunese* and the haptophyte *Emiliania*

71   *huxleyi* (Vardi et al. 1999; Vardi et al. 2009). However most attention has been focused

72   on laboratory systems; cell mortality due to PCD and other types of cell death during

73   natural blooms has been much less studied.

74   Because of their ability to produce potent toxins and therefore cause human

75   poisonings, harmful algal blooms (HABs) have been the subject of intense laboratory and

76   field studies with respect to their ecology, physiology and toxicology (Smayda 1997;

77   Anderson et al. 2005; Erdner et al. 2008). This has resulted in a significant improvement

78   in our understanding of their population dynamics and the underlying processes that lead

79   to the initiation of blooms as well as their subsequent growth and transport pathways. It is

80   generally recognized that populations of benthic life cycle stages or "seedbeds" are key

81   components triggering HAB initiation as they provide the inoculum for blooms

82   (Anderson and Wall 1978; Anderson and Keafer 1985; Garces et al. 2010). These benthic

83   stages can also assist the anthropogenic spread of these organisms, enabling transport

84   under adverse conditions as sometimes occurs in ships' ballast waters or during

85   transplantation of aquaculture animals (Hallegraeff 1993). In some regions, other

86   environmental factors shown to influence bloom formation include enhanced rainfall,

87   freshwater runoff and stabilization of the water column (Therriault et al. 1985; Paerl

88   1997; Weise et al. 2002). As with phytoplankton in general, the causes of HAB decline

89   are less well understood and constrained.

90   In this study, the dinoflagellate *Alexandrium fundyense* (previously identified as *A.*

91   *tamarense* Group I; Lilly et al. 2007; John et al. 2014) was chosen for studying algal

92   bloom dynamics. *A. fundyense* is found in temperate coastal waters worldwide and is a

93   cause of paralytic shellfish poisoning (PSP). For this reason, the physiology, ecology and

94   toxicity of this organism has been investigated extensively in both laboratory and field

95   contexts, making it one of the most well-studied marine unicellular algal species. Past

96   studies have linked the progression of *A. fundyense* blooms to life cycle transitions, from

97   vegetative reproduction during bloom development to sexual fusion and encystment

98   where gametes are formed and fuse to produce a planozygote and later a benthic resting

99   cyst (e.g., Anderson 1998). Quantification of planozygotes during blooms suggests that a

100   significant fraction of the bloom population forms cysts, emphasizing the importance of

101   sexual fusion to bloom termination (Anderson et al. 1983; McGillicuddy et al. 2014;

102   Brosnahan et al. 2015). Other possible contributors to bloom decline include grazing

103   (Petitpas et al. 2015) and parasitism by *Amoebophrya* spp. dinoflagellates (Velo-Suarez

104   et al. 2013). *Amoebophrya* spp. infect *A. fundyense* as free-swimming dinospore cells (~3

105   µm in diameter), then invade the cytosol and nucleus of their host, undergoing multiple

106   rounds of nuclear division and flagellar replication as they form a trophont within the *A.*

107   *fundyense* cell. Maturation of the trophont eventually leads to lysis of the host cell,

108   releasing tens to hundreds of new infective dinospores (Cachon 1964). Similar attack of

109   *A. fundyense* by viruses has not been described, and therefore the role of virus-mediated

110   cell death is unknown. Like many other HABs, the timing and mechanisms involved in

111   the end of *A. fundyense* blooms have considerable socio-economic and ecological

112   implications (Erdner et al. 2008; Anderson 2009). Some HAB species can constitute a

113   large fraction of the phytoplankton biomass during blooms, so cell loss can affect not

114   only community structure and function, but also food web dynamics, toxin dynamics and

115   element cycling.

116   The primary objective of this study was therefore to explore the extent to which cell

117   death processes contribute to *A. fundyense* bloom termination. In particular, we quantified

118   temporal and spatial (depth) changes in natural populations of *A. fundyense* including

119   markers of cell mortality over the course of two inshore blooms. We addressed the role of

120   cell death, in particular PCD, as a contributor to bloom demise and compared its impact

121   as a loss process to infections by *Amoebophrya* parasites. We also placed cell death

122   observations in the context of life cycle transitions by the *A. fundyense* population and

123   evaluated the relative contribution of various loss processes to bloom decline.

124

125   **Materials and methods**

126   **Study sites**

127   The NMS (Nauset Marsh System; Eastham, MA USA) is a network of drowned, tidal

128   kettle ponds connected to each other through shallow, marsh channels and to the Atlantic

129   Ocean via Nauset Inlet (Fig. 1). Salt Pond and Mill Pond are the northern and southern

130   extremities of this system and are significantly deeper than the shallow central marsh area

131   (1.25 m average depth, compared to 9 m and 11 m maximum depths in Salt Pond and

132   Mill Pond, respectively; Crespo et al. 2011). Both ponds experience semidiurnal tides

133   that range from 1-2 meters through the neap-spring cycle. Selective retention of *A.*

134   *fundyense* populations and a north-south temperature gradient across the NMS cause

135   blooms in the two ponds to experience independent development and termination that are

136   staggered in time by 2-3 weeks (Crespo et al. 2011; Ralston et al. 2014). This

137   characteristic of the NMS enabled us to investigate two independent *A. fundyense* blooms

138   through their complete bloom cycle, from development through their peak and

139   termination phases within a single field campaign.

140

141   ***A. fundyense* bloom monitoring**

142   Phytoplankton samples were taken weekly at stations over the deepest areas of Mill Pond

143   (~11 m deep) and Salt Pond (~9 m deep), from early March to late May 2013. Samples

144   were collected during daylight hours and, to the extent possible, near high tide. Actual

145   timing varied due to the logistics associated with accessing the two study locations by

146   land on a single day. Sample times in Mill Pond varied from 10:30 h to 12:00 h and from

147   11:30 h to 14:30 h in Salt Pond. Tidal cycles at these two locations are highly correlated

148   in time and are characterized by rapid floods (~4 h) and slow ebbs (~8 h). Sampling at

149   Salt Pond was always conducted near high water and usually during ebbs so that

150   additional samples could be collected from shallow areas immediately outside Salt Pond

151   for another study. Sampling at Mill Pond was always completed before sampling at Salt

152   Pond and about a third of these latter samples were collected during floods.

153   In Salt Pond, sampling included triplicate 5 L Niskin samples from 1 and 5 m depths

154   and single Niskin samples from depths of 3 m and 1 m above the bottom, over a deep

155   hole, roughly in the center of Salt Pond. In Mill Pond, single 5 L Niskin samples were

156   collected from 1, 3, 5 and 7 m depths as well as 1 m from the bottom, over a deep hole

157   near the northern shore of the pond. *Alexandrium* counts were made from 2 L subsamples

158   of each Niskin collection. These subsamples were concentrated over 20 μm Nitex mesh

159   and fixed with 5% unbuffered formalin in the field before being placed on ice for

160   transport back to the laboratory where they were then resuspended in ice-cold methanol

161   and stored at -20°C until final preparation for counting. Additional 200 mL subsamples

162   were collected from one Niskin bottle at each depth sampled in Salt Pond only for

163   abundance estimation of *Amoebophrya* spp. dinospores. These smaller subsamples were

164   fixed in the field with 2.5% formalin (v/v) and stored on ice for transport to the

165   laboratory where dinospores were concentrated on 0.8 μm polycarbonate filters and

166   serially washed with 50%, 80% and 100% ethanol solutions prior to storage in a -20°C

167   freezer until preparation for counting.

168   Samples for estimation of *A. funydense* abundance were prepared for counting by

169   staining with a species-specific oligonucleotide probe (NA1; 5'-AGT GCA ACA CTC

170   CCA CCA-3') as previously described by Anderson et al. (2005). *Amoebophrya*

171   dinospore abundance was assessed using fluorescence in situ hybridization with tyramide

172   signal amplification (FISH-TSA) as described by Velo-Suarez et al. (2013).

173   The same FISH-TSA protocol was modified as follows to assess infection prevalence

174   in *A. fundyense* host cells that had been fixed and stored as described for abundance

175   estimation using the NA1 oligonucleotide probe. Subsamples of the methanol

176   suspensions containing ~100 cells were concentrated on 0.8 μm polycarbonate filters

177   mounted on a vacuum manifold and without agarose embedding. Samples were left

178   mounted on the manifold, which was used to remove block and stain solutions with

179   minimal manipulation of filters (preventing *A. fundyense* cell loss). This change required

180   the staining solution to be made without addition of dextran sulfate and blocking agent in

181   order to reduce filter clogging. After TSA development, filters were carefully removed

182   from the manifold, mounted on individual slides and stored at 4°C until examination by

183   epifluorescence microscopy. Whole filters were scanned for *A. fundyense* host cells and

184   individual infections were graded 'early' if detectable as a small dot within the host cell,

185   'intermediate' if an *Amoebophrya* cell cluster was present and 'mature' if the parasite had

186   formed a multinuclear trophont.

187

188   **Sampling for PCD markers**

189   Water samples for assessment of PCD markers were collected alongside (and in addition

190   to) samples for *A. fundyense* monitoring with additional samples collected on 9 May and

191   17 May in Salt Pond to better characterize that bloom's termination phase. Whole

192   seawater samples of 4 L were collected using single 5 L Niskin bottles from four discrete

193   depths in Salt Pond: the near-surface (0-1 m), mid-depth (approximately 3 and 5 m) and

194   near-bottom (approximately 7 m), while two depths (5 m and 7 m depths) were chosen

195   for Mill Pond where the maximum concentration of *A. fundyense* cells were typically

196   observed. Samples were immediately stored on ice and brought back to the laboratory for

197   sample processing and analysis. In the laboratory, samples were prescreened with 125 μm

198   and 80 μm pore size sieves to sequentially remove large plankton and detritus, and

199   concentrated by retention of cells on 20 μm Nitex mesh. Cells were then backwashed

200   with filtered seawater to a final volume of 30 mL and triplicate 1 mL aliquots were

201   prepared for observation of viability, PCD, ROS markers and for cell size assessments.

202   Three, 1 mL aliquots were also taken from each PCD marker sample, preserved with

203   Lugol's iodine solution (1% final concentration), and counted using a 1mL Sedgewick-

204   Rafter counting chamber to provide additional *A. fundyense* cell abundance estimates

205   alongside cell counts from separate Niskin samples used for the bloom monitoring.

206

207   *A. fundyense* **viability assay**

208   Cell viability was evaluated using both Evans Blue (final concentration of 1:2000 (w/v)

209   of 1% stock (w/v)) (Crippen and Perrier 1974) and Zombie Aqua (BioLegend, San

210   Diego, CA USA) according to the manufacturers' instructions. Cells with intact plasma

211   membranes exclude the Evans Blue dye, whereas the dye penetrates and stains dead cells.

212   Zombie Aqua reacts with primary amine groups on proteins, and dead cells show

213   increased protein labeling as the dye penetrates into the cytoplasm while live cells are

214   only labeled with surface proteins. An advantage of the Zombie Aqua dye is that live-

215   dead determinations can be made after fixation, enabling postponement of analysis for

216   some time after treatment. In contrast, cells treated with Evans Blue need to be analyzed

217   within a few hours to ensure accurate viability estimates. In both assays, cell viability was

218   assessed from three 1 mL subsamples using a Zeiss Axioskop epifluorescence

219   microscope outfitted with a DAPI/Hoeschst filter set (excitation wavelength 365/50 nm

220   and emission of 445/50 nm).

221

222   **In situ detection of PCD markers**

223   A distinctive feature of PCD is the activation of caspase enzymes. Caspase activity was

224   assayed with Image-iT™ LIVE Green Poly Caspases Detection Kit (Invitrogen,

225   Carlsbad, CA USA), which is based on a fluorescent inhibitor of caspases (FLICA™).

226   Cells were harvested by centrifugation at $1000 \times g$ for 5 min, resuspended in 1X FLICA

227   working reagent, and incubated for 60 min at room temperature in darkness. Cells were

228   washed twice with wash buffer and fixed before analyzing under a Zeiss Axioskop

229   epifluorescence microscope outfitted with a FITC filter set (excitation wavelength 470/40

230   nm and emission of 525/50 nm). Measurements from each sample were made from three

231   1 mL aliquots.

232

233   **ROS detection assay**

234   Levels of intracellular reactive oxygen species (ROS), known mediators for PCD, were

235   measured using the oxidation-sensitive fluorescent probe, carboxy-H_2DCFDA [5-(and 6)-

236   carboxy-2',7'-dichlorodihydrofluorescein diacetate] (Invitrogen, Carlsbad, CA USA).

237   Aliquots (1 mL) of samples were centrifuged at $1000 \times g$ for 5 min. The supernatant was

238   carefully discarded, and the pellet was resuspended in 1 mL of 10 mM PBS buffer, pH

239   7.5 containing a final concentration of 5 μM H_2DCFDA and incubated for 60 min at 20˚C

240   in darkness. Cells were then washed twice with PBS. Green DCF fluorescence of cells

241   was observed with a Zeiss Axioskop epifluorescence microscope equipped with a FITC

242   filter set (excitation wavelength 470/40 nm and emission of 525/50 nm).

243

244   **Measurement of *A. fundyense* cell size distributions**

245   *A. fundyense* cells fixed with 5% unbuffered formalin were captured from random fields

246   of view, and the number of cells and their areas were estimated using ImageJ software

247   (National Institute of Health, Bethesda, MD USA) following a protocol for single cell

248   area measurements outlined by Papadopulos et al. (2007). Briefly, measurements from

11

249   cell images collected under 200x magnification were calibrated according to a 20 μm

250   standard under the same magnification. Cell sizes were determined automatically using

251   the "Analyze Particles" function in ImageJ, which applied an automated threshold for

252   detection of cell boundaries and calculated minimum, maximum and equivalent spherical

253   diameters. In turn, individual cell volumes were estimated using a spherical

254   approximation. Cell size was used as an indicator of life cycle stage following criteria

255   applied by Brosnahan et al. (2015). Late-stage planozygotes were defined as large cells

256   greater than 43 μm in an equivalent circular diameter based on previous descriptions

257   (Anderson et al. 1983), and gametes were defined as cells smaller than 30 μm in an

258   equivalent circular diameter (Brosnahan et al. 2015). This corresponds to the smallest 5%

259   of cell volumes observed in samples from the start of the *A. fundyense* bloom in Salt

260   Pond (sample collected 22 April). Partitioning of the population into gamete, vegetative

261   cell and late-stage planozygotes was then assessed by determining the proportion with

262   volumes $<14,137 \ \mu m^3$, $>14,137 \ \mu m^3$ and $<41,630 \ \mu m^3$, and $>41,630 \ \mu m^3$, respectively.

263

264   **Results**

265   *A. fundyense* **population dynamics in Mill Pond and Salt Pond**

266   Our results from the overall water column analysis revealed that *A. fundyense* was the

267   dominant phytoplankton species and the maximum cell concentrations were mostly

268   observed in subsurface samples - either from 3 or 5 m depth in Salt Pond and 5 or 7 m

269   depth in Mill Pond - and surface cell concentrations remained low throughout the bloom

270   period (Fig. 2). We used depth samples where the maximum cell numbers were observed

271   as the most representative sample for the *A. fundyense* population in both ponds. At the

272   beginning of the sampling period (25 March), the bloom had already started in Mill Pond

273   as *A. fundyense* mean concentration was greater than ~6,000 cells L^{-1} at 7 m depth (data

274   not shown). *A. fundyense* concentrations continued to increase until the bloom peaked on

275   29 April with maximum concentrations of ~2.2×10^6 cells L^{-1}, about a month after the first

276   sampling period. Subsequently, cell abundance decreased about 6-fold (~3.5×10^5 cells L$^-$

277   ^{1}) over the next week and dramatically declined >350-fold the following week to ~1,000

278   cells L^{-1} (Fig. 2a).

279   The peak of the bloom in Salt Pond was nearly two weeks later than the Mill Pond

280   peak (9 May vs. 29 April in Mill Pond), however development of the bloom was much

281   faster than Mill Pond (1 Apr - 29 Apr in Mill Pond vs. 22 Apr - 9 May in Salt Pond).

282   Concentrations of *A. fundyense* in Salt Pond peaked on 9 May, reaching ~1×10^6 cells L^{-1}.

283   *A. fundyense* concentrations decreased dramatically over the next week (9-17 May),

284   declining 66-fold (to ~15,000 cells L^{-1}) on 17 May and remaining less than 1,000 cells L^{-1}

285   through the end of the sampling period.

286

287   **Cell death, PCD and infections in *A. fundyense***

288   Less than 5% dead cells were detected during the development phase including the peak

289   of the blooms in both Mill and Salt Ponds. However, in Mill Pond over 10% dead cells

290   were observed during termination (6 May, 14.1% at 7 m depth). Fewer dead cells were

291   observed a week later, though overall *A. fundyense* abundance was down as well (13

292   May, 8.3% at 5 m depth, ~1,000 cells L^{-1}; Fig. 3a). A similar but less intense pattern of

293   cell mortality was observed in Salt Pond where very few dead cells were detected up to

294   the peak of the bloom. Dead cells then increased as a proportion of the population during

295   termination (6.8% on 13 May and 5.5% on 17 May at 5 m depth; Fig. 3b). Caspase

296   activity was measured only in Salt Pond, where active caspase levels increased in parallel

297   with dead cells after the bloom's peak (Fig. 3b).

298   Another common feature of PCD is intracellular ROS production, which serves as a

299   trigger for cell death. Cells exhibiting endogenous ROS generation were observed about

300   two weeks prior to the bloom peak both in Mill Pond and Salt Pond, but were barely

301   detected otherwise (Fig. 3a and 3b). An exception was the end of the bloom in Salt Pond,

302   where cells showed a dramatic increase in ROS generation ($35.5 \pm 3.0\%$ on 17 May at 5

303   m depth) on our last sampling date (Fig. 3b).

304   In Salt Pond, *Amoebophrya* dinospores were observed throughout the bloom period

305   and their abundance remained relatively constant until the bloom's termination when

306   dinospore abundance increased sharply. This spike in dinospore abundance was preceded

307   by a similar increase in the prevalence of *Amoebophrya* infections near the bloom's peak.

308   Prevalence estimates from earlier in the bloom's development were less than 5% for all

309   infection stages, but increased to a combined 26.7% after the bloom's peak (Fig. 3c). The

310   impact of parasitic infections and cell death was further examined over depth (Fig. 3d).

311   Prior to the bloom peak, higher infection rates were observed at 3 m than at 5 m on 29

312   Apr and 6 May (5.8% and 13.1% at 3 m and 3.3% and 7.1% at 5 m depth, respectively).

313   Similarly, increased numbers of dead cells were found at 3 m than at 5 m depth although

314   the prevalence of infections was higher than the proportions of dead cells. A distinct

315   depth distribution was observed during bloom decline (13 May) when infections were

316   more prevalent at 5 m (26.7%) than at 1 m (13.5%), but dead cells were proportionally

317   more abundant closer to the surface (26.8% at 1 m compared to 5.0% at 3 m and 6.8% at

318   5 m; Fig. 3d).

319

320   **Cell size distributions over the course of the *A. fundyense* bloom in Salt Pond**

321   *A. fundyense* cell sizes were measured and compared over the bloom period to track cells

322   potentially representing three distinct life-cycle stages - vegetative cells, gametes and

323   planozygotes - based on their size. Though vegetative cell size varies over the light:dark

324   cycle in natural populations (e.g. Brosnahan et al. 2015), sexual life cycle transitions are

325   clearly recognizable from large shifts in bloom populations toward smaller (gamete) and

326   larger (mature planozygote) cells (Fig. 4a and Supplementary Fig. S1). During the early

327   phase of the bloom in Salt Pond, the *A. fundyense* population was dominated by

328   vegetative cells (96.4%), volumes between 14,172 μm^3 and 36,998 μm^3 (mean: 22,848.7

329   μm^3, 22 Apr; Supplementary Table S1 and Fig. 4b). Small and large cells, gametes and

330   late-stage planozygotes respectively, were also detected at this time, but were each less

331   than 4% of the total population and therefore were more likely especially large and small

332   mitotic stages (3.2% gametes, cells smaller than 14,137 μm^3 and 0.4% planozygotes, cells

333   larger than 41,630 μm^3). As the bloom continued to develop, the population remained

334   dominated by vegetative cells with 84% of cells still within the vegetative cell size range

335   (29 Apr). Mean cell size continued to decrease until the peak of the bloom where most

336   cell sizes were less than 20,000 μm^3 with a mean size of 12744.1 μm^3 on 9 May - roughly

337   half of the mean cell volume measured on 22 April (Supplementary Table S1). Very

338   small cells (less than 10,000 μm^3) were over 47% of the population at this time

339   (Supplementary Figure S1). The mean cell size in the population then increased abruptly,

15

340   with a mean size of 27091.9 μm^3 as the bloom declined (13 May). The mean cell size

341   continued to increase up to 32987.4 μm^3 at the end of the bloom (Supplementary Table

342   S1 and Fig. 4a). While most of these post bloom peak cells were classified as vegetative

343   cells by our size criteria, they are more likely to have been early stage planozygotes,

344   which can be comparable in size to vegetative cells (Brosnahan et al. 2014; Brosnahan et

345   al. 2015).

346

347   **Discussion**

348   **Evidence of cell death during *A. fundyense* bloom decline**

349   Over the past decade, concepts of phytoplankton cell death have evolved rapidly with the

350   discovery that phytoplankton often die spontaneously through processes independent

351   from grazing and sedimentation (Franklin et al. 2006; Berges and Choi 2014). Cell

352   mortality caused by PCD has received more attention since accumulating physiological

353   and biochemical data collectively suggest that PCD is triggered by diverse environmental

354   cues, often when phytoplankton encounter adverse environmental conditions (Bidle and

355   Falkowski 2004). The presence of an operational PCD molecular machinery, e.g.

356   metacaspases in phytoplankton genomes, indicates PCD was established early in the

357   evolution of unicellular phytoplankton and therefore is potentially important for

358   phytoplankton bloom dynamics (Choi and Berges 2013). However, the role of PCD has

359   not been widely examined in natural populations. The one other study of which we are

360   aware focused on an *E. huxleyi* bloom where PCD was associated with the spread of viral

361   infections (Vardi et al. 2012). Our study uniquely has assessed the occurrence of PCD

362   and other cell death through the full course of an algal species' bloom cycle, from its

363   development through its demise and contrasts the impact of cell death on bloom demise

364   to that of other loss pathways, particularly infections by an intracellular parasite

365   (*Amoebophrya* spp.) that chronically impacts inshore dinoflagellate blooms.

366   Cell mortality was quantified in an effort to understand the role of cell death in bloom

367   dynamics, particularly its contribution to the termination of blooms of the toxic

368   dinoflagellate *A. fundyense*. Dead cells were barely detected during the early phase of

369   development through bloom peaks, indicating that most cells were actively growing.

370   Increases in cell mortality were observed only after *A. fundyense* cell abundance had

371   already declined sharply. The highest proportions of dead cells measured in the Mill Pond

372   and Salt Pond populations were between 5 and 15% (Fig. 3a and 3b). These results

373   indicate that cell death was a significant cell loss pathway during the late stages of both

374   *A. fundyense* blooms recorded. In particular, we observed *A. fundyense* cells exhibiting

375   features of PCD (intracellular ROS generation and caspase activity) during bloom

376   decline, suggesting the presence of PCD as a cell death pathway in *A. fundyense*. Genes

377   encoding metacaspases, molecular executioners that initiate PCD processes, are found in

378   *Alexandrium* species (Choi et al. manuscript in prep), and increased metacaspase activity

379   was observed under stressful conditions suggesting the presence of PCD in *A. fundyense*

380   (Jauzein and Erdner 2013).

381   Interestingly, a drastic increase in ROS level was detected at the end of the bloom

382   period in Salt Pond (Fig. 3a and 3b), indicating that *A. fundyense* cells were stressed. In

383   other systems ROS generation has been associated with active host defense against

384   parasite infection (Lu et al. 2014). The *A. fundyense* in Salt Pond were also observed to

385   suffer from *Amoebophrya* infections at the end of the bloom, with infection prevalence

386 comparable to observations made during the previous year's bloom (Velo-Suarez et al.

387 2013). However, in Mill Pond where infections were also observed, though with lower

388 prevalence, a similar ROS spike was not observed. The Mill Pond population may have

389 had a lesser parasite challenge than the Salt Pond population or a parasite-associated ROS

390 spike in Mill Pond was simply missed by our sampling. Increased ROS generation was

391 also observed in both Mill and Salt Ponds during bloom development - about two weeks

392 before each bloom's peak - without noticeable cell death and only minimal levels of

393 parasitism. It is not clear what triggered these earlier elevated ROS levels, since no spikes

394 in dinospore abundance or cell infections were observed at those times (Fig. 3c). ROS

395 production has also been shown to increase during bloom development in *Peridinium* due

396 to CO_2 limitation (Vardi et al. 1999), underscoring its generalized association with stress

397 on algal cells. Our results suggest that *A. fundyense* may experience transient stressful

398 conditions during rapid growth, but such conditions, at least in the case of these blooms,

399 did not slow bloom development to an appreciable extent.

400

401 **Other sources of cell loss**

402 Cell death is just one of many loss processes that contribute to *A. fundyense* bloom

403 termination. For phytoplankton generally, grazing, viral lysis and parasite infection are

404 recognized sources of mortality. In the case of *A. fundyense*, life cycle transitions have

405 been shown to play a major role in the termination of both inshore and offshore blooms,

406 specifically the shift from vegetative reproduction during the early phase of blooms to

407 sexual encystment, a process which begins when gametes are formed and ends when new

408   zygotic resting cysts are recruited to the ocean bottom (Anderson et al. 1983;

409   McGillicuddy et al. 2014; Brosnahan et al. 2015).

410   It has been difficult to quantify the different life cycle stages, since vegetative cells,

411   gametes and planozygotes are morphologically similar to one another, but work by

412   Brosnahan et al. (2015) directly linked the production of small cells with gametogenesis

413   in Salt Pond. In this study, cell size data is used to estimate the impact of life cycle

414   transitions on the 2013 bloom in Salt Pond (Fig. 4, Supplementary Table S1 and

415   Supplementary Fig. S1). The gamete size range was defined as the smallest 5% of cells

416   (<30 μm equivalent circular diameter, <14,137 μm^3 in volume) present at the start of the

417   bloom, when the population was composed almost exclusively of vegetative cells. Late-

418   stage planozygotes were also identified based on their size, i.e. as cells whose equivalent

419   circular diameter was greater than 43 μm (estimated volume was >41,630 μm^3). Both of

420   these size-based definitions agree well with those established by Brosnahan et al. (2015)

421   from analysis of *A. fundyense* images recorded by an Imaging FlowCytobot. An

422   important limitation of this size-based approach is that it misclassifies early-stage

423   planozygotes as vegetative cells. It's very likely that most vegetative size-class cells

424   present after the bloom's peak were in fact early-stage planozygotes (Brosnahan et al.

425   2015).

426   Based on the cell size changes recorded, the proportion of vegetative cells, gametes

427   and late-stage planozygotes was estimated for each sampling day over the full course of

428   the bloom in Salt Pond (Fig. 4b). During the bloom's development, our size criteria

429   classified over 96% of *A. fundyense* as vegetative cells, consistent with prior work that

430   has shown bloom formation in this system to be driven by division rather than cyst

431   germination (Crespo et al. 2011). While maximum and minimum cell sizes indicated that

432   both gametes and planozygotes were also present during bloom development, this is more

433   likely classification error associated with ongoing mitotic cell division. As the bloom

434   matured, the proportion of vegetative cells decreased markedly, comprising less than

435   40% of the population at the bloom peak on 9 May (36.1%; Fig. 4b). During the bloom's

436   subsequent decline, the proportion of gametes then dropped drastically, suggesting a

437   significant loss of cells through mating (Fig. 4b).

438   In contrast to encystment, grazing - though a major loss pathway for other

439   phytoplankton species - appears to have minimal impacts on *A. fundyense* within the

440   Nauset Marsh System. While the grazer community consuming *A. fundyense* is diverse

441   and includes several meso- and microplankton (ciliates, rotifers, heterotrophic

442   dinoflagellates, copepod stages and marine cladocerans; Turner and Anderson 1983;

443   Petitpas et al. 2015) and filter-feeding animals (clams, mussels and oysters), combined

444   loss rates to these grazer populations have been challenging to quantify. Recent work in

445   Salt Pond by Petitpas et al. (2015) showed that grazing did not appear to hinder net

446   growth by *A. fundyense* during bloom development. Similarly, continuous in situ imaging

447   flow cytometry applied by Brosnahan et al. (2015) showed that accumulation of *A.*

448   *fundyense* was comparable to an estimator of the population's in situ division rate,

449   supporting the contention that grazing only minimally impacts the *A. fundyense*

450   population in Salt Pond.

451   Inshore populations of *A. fundyense* are also known to be chronically impacted by

452   *Amoebophrya* spp. parasites. In this study, the proportion of infected cells remained low

453   through the peak of both blooms but increased afterwards, up to a maximum of 26.7%

454   combined for all stages of infection in Salt Pond (Fig. 3c). The temporal pattern and

455   intensity of parasite impact on the bloom was highly similar to the 2012 Salt Pond bloom

456   which had maximum infection prevalence of about 30% during its termination (Velo-

457   Suàrez et al. 2013). Across all samples collected, maximum infection rates were higher

458   than the observed proportion of dead cells, and the proportions of dead cells and infected

459   cells showed contrasting patterns with depth (Fig. 3d). Given these differences in their

460   distribution, we disregard the possibility that some cell death positive cells were also

461   infected by the parasite and instead consider parasite infection and mortality as distinct

462   cell loss pathways.

463

464   **Relative contribution of loss processes to bloom declines**

465   Our results indicate that parasite infection, cell death and gametogenesis are all pathways

466   for cell loss during the observed *Alexandrium* blooms. Cell numbers in Salt Pond

467   declined precipitously after the bloom peak, with a reduction of 87% between 9 and 13

468   May, and then 88% of the remainder by 17 May (98% of 9 May population). How much

469   of these losses are attributable to cell death, parasitism, life cycle transitions and other

470   processes such as grazing?

471   Loss rates from cell death can be estimated from the proportion of cells in a particular

472   state divided by that state's persistence time. In the case of cells infected by

473   *Amoebophyra* spp., the persistence time depends on their stage of infection (Velo-Suarez

474   et al. 2013). For dead cells, persistence can be estimated from cell settling times. While

475   settling time has not been measured directly from dead *A. fundyense* cells, measured

476   settling rates of other comparably sized dinoflagellates are 2-3 m d^{-1} (Kamykowski et al.

477   1992). Given mean depths across the two NMS ponds, this translates to persistence times

478   of less than half a day. In a sample where 7% of the cells are dead, we estimate that cell

479   death is causing population declines of at least 14% day^{-1}.

480   For losses to sexual fusion and encystment, the persistence time might correspond to

481   how long a gamete might take to fuse with a second gamete to form a planozygote and

482   then encyst. However, mounting evidence suggests that some planozygotes may divide to

483   regenerate gamete sized cells, complicating a similar, simple adaptation of the persistence

484   time model for estimating encystment losses (Brosnahan et al. 2015; Figueroa et al. 2015)

485   Still, the concerted nature of the bloom's sexual transition is useful for considering what

486   fraction each loss process might contribute to the total decline of the Salt Pond bloom.

487   Through its rapid transition to sexual stages, the bloom essentially stops division,

488   enabling us to ignore population growth after the bloom's peak (Brosnahan et al. 2015).

489   Loss rates from various processes are therefore directly translatable to the total

490   contribution each makes to the blooms' ultimate demise.

491   We used a simple model to calculate the daily and total loss of cells due to parasitism

492   and cell death during bloom decline. We have observations from 9, 13 and 17 May, and

493   we extrapolated the cell numbers in between by applying an exponential loss curve. The

494   proportion of infected cells was interpolated linearly between observations, and we used

495   the same approach for the estimation of cell mortality. For example, the 2.1% dead cells

496   on 9 May was interpolated linearly to the 28.6% dead cells measured on 13 May and

497   similarly for the interval from 13 May to 17 May. From these approximations, we

498   calculated daily loss contributions from each process to the bloom's overall decline.

499   These calculations are provided in Supplementary Table S2.

500　　　Between 9 and 13 May, *A. fundyense* concentrations decreased by about an order of

501　　magnitude, daily loss due to infection ranged from 8.8 to 23.4% day^{-1} with a cumulative

502　　contribution of 12.7% of the peak bloom population. Daily loss rates due to cell death

503　　ranged from 9.9 to 52.9% day^{-1}, and cumulative loss rate was 21.4%. The remaining

504　　65.9% of peak population loss is attributed primarily to encystment but other factors

505　　(e.g., grazing and dispersal) also likely contributed. Later during the Salt Pond bloom's

506　　decline, between 13 and 17 May, cell numbers were greatly reduced but still high (10^4-

507　　10^5 L^{-1}) and cell death and parasitism played a more significant role in the overall loss

508　　rate with maximum daily losses of 37.8% to parasitism and 61.6% to cell death.

509　　　Combined, cell death and *Amoebophrya* infection account for 42.5% of the bloom's

510　　total decline. An important caveat to this estimate is that the calculations are highly

511　　sensitive to our underlying assumptions, especially regarding interpolation of cell death

512　　and infection rates between sparse data. While these processes certainly have the

513　　potential to play major roles in the demise of *A. fundyense* blooms, the high estimate of

514　　parasite-induced loss contradicts a recent, intensive study of this same system through

515　　which higher maximum infection rates were observed but the total fraction of the

516　　population succumbing to infection was estimated to be much lower (Velo-Suarez et al.

517　　2013). Similar intensive studies of cell death that better sample the spatial and temporal

518　　patchiness of this process may significantly alter our understanding of the role played by

519　　cell death on the demise of *A. fundyense* and other harmful algal blooms.

520　　　In all, mating and cyst formation appears to be the dominant process for bloom decline

521　　in the Salt Pond system, both in this study (2013) and in 2012 (Brosnahan et al. 2015).

522　　This is based upon the rapid synchronous appearance of gametes right before the bloom

523   peak, coupled with their rapid disappearance immediately afterwards. However, while the

524   gametes undoubtedly disappear from the water column, their ultimate fate is unclear.

525   Planozygote proportions do not increase concurrently or in proportion to gamete

526   disappearance (Fig. 4b; Brosnahan et al. 2015). This could result from rapid encystment,

527   i.e. a short residence time in the pond water column as planozygotes, but post-bloom

528   estimates of cyst abundance within the pond only account for about 10% of the bloom's

529   peak (M.L. Brosnahan unpubl. data). Shoaling of vertical swimming ambits was also

530   observed during the 2013 bloom's sexual transition, suggesting that export from the pond

531   is likely heightened during the bloom's sexual phase. Post-bloom numbers of cysts within

532   the pond therefore likely grossly underestimate the true conversion of the population to

533   sexual stages and retention within Salt Pond may differ between different *A. fundyense*

534   sexual stages (Brosnahan et al. manuscript in prep). More detailed descriptions of export

535   of sexual stage cells is likely to further alter the estimated impacts of cell death and other

536   processes on bloom decline since the calculation described here ignores the possibility

537   that dead cells might be exported from the pond at higher rates than e.g. infected cells,

538   which tended to be distributed deeper in the pond.

539   Impacts from loss processes besides encystment - parasitism, grazing and cell death -

540   appear to become the main cell loss pathways after the bloom's peak, and therefore after

541   the bulk of the population likely underwent encystment. Adverse conditions trigger

542   encystment of *Alexandrium* in the lab (Anderson et al. 1984), and stressors can induce

543   temporary cysts in clonal culture (Jauzein and Erdner 2013). Thus, *Alexandrium* may be

544   able to avoid adverse conditions by encysting, with other loss processes operating

545   primarily on those cells that are unable to find a mating partner or are slow to mature as

546   planozygotes. It is also likely that the relative contribution of different loss factors varies

547   depending on the environment. Salt Pond is a relatively contained system where blooms

548   reach very high densities, which should enhance the probability of both gamete

549   encounters and propagation of parasitic infections. In larger, more open systems where

550   blooms typically achieve lower peak cell concentrations, the probability of encountering

551   a compatible gamete may be reduced, increasing the likelihood of cell death or other

552   fates.

553

554   **Conclusions**

555   Our results indicate that *A. fundyense* cells undergo endogenous cell death, potentially via

556   PCD pathways, during bloom decline. This adds natural cell death as an additional source

557   of cell loss during *A. fundyense* blooms. In the relatively small and contained Salt Pond

558   system, life cycle transitions (i.e., cyst formation) appear to be the biggest contributor to

559   bloom decline, followed by cell death, parasitism and other processes such as grazing.

560   Unlike other phytoplankton that undergo cell death when exposed to adverse conditions,

561   some dinoflagellates including *A. fundyense* can overcome adverse conditions via

562   encystment, so cell death and parasitism may represent the ultimate fates only for those

563   cells that do not manage to successfully complete this life cycle transition. Understanding

564   bloom decline is a high priority with implications for HAB control and prevention, and

565   our results not only contribute significantly to our knowledge of phytoplankton bloom

566   dynamics, but provide a framework for studying other blooms.

567

568   **References**

569   Anderson, D., S. Chisholm, and C. Watras. 1983. Importance of life cycle events in the

570   population dynamics of *Gonyaulax tamarensis*. Mar. Biol. **76:** 179-189.

571   doi:10.1007/BF00392734

572   Anderson, D., D. Townsend, D. McGillicuddy, and J. Turner. 2005. The ecology and

573   oceanography of toxic *Alexandrium fundyense* blooms in the Gulf of Maine. Deep

574   Sea Res., Part II **52:** 2365-2368. doi:10.1016/j.dsr2.2005.08.001

575   Anderson, D. M. 1998. Physiology and bloom dynamics of toxic *Alexandrium* species,

576   with emphasis on life cycle transitions. Nato ASI Ser., Ser. G **41:** 29-48.

577   Anderson, D. M. 2009. Approaches to monitoring, control and management of harmful

578   algal blooms (HABs). Ocean Coast. Manage. **52:** 342-347.

579   doi:10.1016/j.ocecoaman.2009.04.006

580   Anderson, D. M., and B. A. Keafer. 1985. Dinoflagellate cyst dynamics in coastal and

581   estuarine waters, p. 219-224. Anderson DM, White AM, and Baden DG [eds.],

582   Toxic Dinoflagellates. New York: Elsevier.

583   Anderson, D. M., D. M. Kulis, and B. J. Binder. 1984. Sexuality and cyst formation in

584   the dinoflagellate *Gonyaulax tamarensis*: cyst yield in batch cultures. J. Phycol.

585   **20:** 418-425. doi:10.1111/j.0022-3646.1984.00418.x

586   Anderson, D. M., and D. Wall. 1978. Potential importance of benthic cysts of *Gonyaulax*

587   *tamarensis* and *G. excavata* in initiating toxic dinoflagellate blooms. J. Phycol.

588   **14:** 224-234. doi:10.1111/j.1529-8817.1978.tb02452.x

589   Berges, J. A., and C. J. Choi. 2014. Cell death in algae: physiological processes and

590   relationships with stress. Perspect. Phycol. **1:** 103-112.

591   doi:10.1127/pip/2014/0013

592   Berges, J. A., and P. G. Falkowski. 1998. Physiological stress and cell death in marine

593   phytoplankton: induction of proteases in response to nitrogen or light limitation.

594   Limnol. Oceanogr. **43:** 129-135. doi:10.4319/lo.1998.43.1.0129

595   Bidle, K. D., and S. J. Bender. 2008. Iron starvation and culture age activate

596   metacaspases and programmed cell death in the marine diatom *Thalassiosira*

597   *pseudonana*. Eukaryotic Cell **7:** 223-236. doi:10.1128/ec.00296-07

598   Bidle, K. D., and P. G. Falkowski. 2004. Cell death in planktonic, photosynthetic

599   microorganisms. Nat. Rev. Microbiol. **2:** 643-655. doi:10.1038/nrmicro956

600   Brosnahan, M. L., S. Farzan, B. A. Keafer, H. M. Sosik, R. J. Olson, and D. M.

601   Anderson. 2014. Complexities of bloom dynamics in the toxic dinoflagellate

602   *Alexandrium fundyense* revealed through DNA measurements by imaging flow

603   cytometry coupled with species-specific rRNA probes. Deep Sea Res., Part II

604   **103:** 185-198. doi:10.1016/j.dsr2.2013.05.034

605   Brosnahan, M. L. and others 2015. Rapid growth and concerted sexual transitions by a

606   bloom of the harmful dinoflagellate *Alexandrium fundyense* (Dinophyceae).

607   Limnol. Oceanogr. **60:** 2059-2078. doi:10.1002/lno.10155

608   Brussaard, C. P. 2004. Viral control of phytoplankton populations - a Review. J.

609   Eukaryotic Microbiol. **51:** 125-138. doi:10.1111/j.1550-7408.2004.tb00537.x

610   Cachon, J. 1964. Contribution à l'étude des péridiniens parasites. Cytologie, cycles

611   évolutifs. Ann. Sci. Nat. Zool **6:** 1-158.

612   Calbet, A., and M. R. Landry. 2004. Phytoplankton growth, microzooplankton grazing,

613   and carbon cycling in marine systems. Limnol. Oceanogr. **49:** 51-57.

614   doi:10.4319/lo.2004.49.1.0051

615 Chambouvet, A., P. Morin, D. Marie, and L. Guillou. 2008. Control of toxic marine

616   dinoflagellate blooms by serial parasitic killers. Science **322:** 1254-1257.

617   doi:10.1126/science.1164387

618 Choi, C. J., and J. A. Berges. 2013. New types of metacaspases in phytoplankton reveal

619   diverse origins of cell death proteases. Cell Death Dis. **4:** e490.

620   doi:10.1038/cddis.2013.21

621 Cloern, J. E. 1996. Phytoplankton bloom dynamics in coastal ecosystems: A review with

622   some general lessons from sustained investigation of San Francisco Bay,

623   California. Rev. Geophys. **34:** 127-168. doi:10.1029/96rg00986

624 Crespo, B. G., B. A. Keafer, D. K. Ralston, H. Lind, D. Farber, and D. M. Anderson.

625   2011. Dynamics of *Alexandrium fundyense* blooms and shellfish toxicity in the

626   Nauset Marsh System of Cape Cod (Massachusetts, USA). Harmful Algae **12:** 26-

627   38. doi:10.1016/j.hal.2011.08.009

628 Crippen, R., and J. Perrier. 1974. The use of neutral red and evans blue for live-dead

629   determinations of marine plankton (with comments on the use of rotenone for

630   inhibition of grazing). Biotech. Histochem. **49:** 97-104.

631   doi:10.3109/10520297409116949

632 Erdner, D. L. and others 2008. Centers for oceans and human health: a unified approach

633   to the challenge of harmful algal blooms. Environ. Health **7** (Suppl. 2): S2.

634   doi:10.1186/1476-069x-7-s2-s2

635 Figueroa, R. I., C. Dapena, I. Bravo, and A. Cuadrado. 2015. The hidden sexuality of

636   *Alexandrium minutum*: An example of overlooked sex in dinoflagellates. Plos

637   One **10:** e0142667. doi:10.1371/journal.pone.0142667

638 Franklin, D. J., C. P. D. Brussaard, and J. A. Berges. 2006. What is the role and nature of

639 programmed cell death in phytoplankton ecology? Eur. J. Phycol. **41:** 1-14.

640 doi:10.1080/09670260500505433

641 Garces, E., M. Montresor, J. Lewis, K. Rengefors, D. M. Anderson, and H. Barth. 2010.

642 Phytoplankton life cycles and their impacts on the ecology of harmful algal

643 blooms. Deep Sea Res., Part II **57:** 159-161. doi:10.1016/j.dsr2.2010.01.002

644 Hallegraeff, G. M. 1993. A review of harmful algal blooms and their apparent global

645 increase. Phycologia **32:** 79-99. doi:10.2216/i0031-8884-32-2-79.1

646 Jauzein, C., and D. L. Erdner. 2013. Stress-related responses in *Alexandrium tamarense*

647 cells exposed to environmental changes. J. Eukaryotic Microbiol. **60:** 526-538.

648 doi:10.1111/jeu.12065

649 John, U., R. W. Litaker, M. Montresor, S. Murray, M. L. Brosnahan, and D. M.

650 Anderson. 2014. Formal revision of the *Alexandrium tamarense* species complex

651 (Dinophyceae) taxonomy: The introduction of five species with emphasis on

652 molecular-based (rDNA) classification. Protist **165:** 779-804.

653 doi:10.1016/j.protis.2014.10.001

654 Kamykowski, D., R. E. Reed, and G. J. Kirkpatrick. 1992. Comparison of sinking

655 velocity, swimming velocity, rotation and path characteristics among six marine

656 dinoflagellate species. Mar. Biol. **113:** 319-328. doi:10.1007/BF00347287

657 Lilly, E. L., K. M. Halanych, and D. M. Anderson. 2007. Species boundaries and global

658 biogeography of the *Alexandrium tamarense* complex (Dinophyceae). J. Phycol.

659 **43:** 1329-1338. doi:10.1111/j.1529-8817.2007.00420.x

660   Lu, Y., S. Wohlrab, G. Glöckner, L. Guillou, and U. John. 2014. Genomic insights into

661   processes driving the infection of *Alexandrium tamarense* by the parasitoid

662   *Amoebophrya sp*. Eukaryotic Cell **13**: 1439-1449. doi:10.1128/ec.00139-14

663   McGillicuddy, D. J. and others 2014. A red tide of *Alexandrium fundyense* in the Gulf of

664   Maine. Deep Sea Res., Part II **103:** 174-184. doi:10.1016/j.dsr2.2013.05.011

665   Papadopulos, F. and others 2007. Common tasks in microscopic and ultrastructural image

666   analysis using ImageJ. Ultrastruct. Pathol. **31: ** 401-407. doi:

667   10.1080/01913120701719189

668   Paerl, H. W. 1997. Coastal eutrophication and harmful algal blooms: Importance of

669   atmospheric deposition and groundwater as "new" nitrogen and other nutrient

670   sources. Limnol. Oceanogr. **42:** 1154-1165.

671   doi:10.4319/lo.1997.42.5_part_2.1154

672   Petitpas, C. M., J. T. Turner, B. A. Keafer, D. J. McGillicuddy, and D. M. Anderson.

673   2015. Zooplankton community grazing impact on a toxic bloom of *Alexandrium*

674   *fundyense* in the Nauset Marsh System, Cape Cod, Massachusetts, USA. Harmful

675   Algae **47:** 42-55. doi:10.1016/j.hal.2015.05.010

676   Ralston, D. K., B. A. Keafer, M. L. Brosnahan, and D. M. Anderson. 2014. Temperature

677   dependence of an estuarine harmful algal bloom: Resolving interannual variability

678   in bloom dynamics using a degree-day approach. Limnol. Oceanogr. **59:** 1112-

679   1126. doi:10.4319/lo.2014.59.4.1112

680   Segovia, M. A., L. Haramaty, J. A. Berges, and P. G. Falkowski. 2003. Cell death in the

681   unicellular chlorophyte *Dunaliella tertiolecta*. A hypothesis on the evolution of

682   apoptosis in higher plants and metazoans. Plant Physiol. **132:** 99-105.

683   doi:10.1104/pp.102.017129

684 Smayda, T. J. 1997. Harmful algal blooms: Their ecophysiology and general relevance to

685   phytoplankton blooms in the sea. Limnol. Oceanogr. **42:** 1137-1153.

686   doi:10.4319/lo.1997.42.5_part_2.1137

687 Therriault, J., J. Painchaud, and M. Levasseur. 1985. Factors controlling the occurrence

688   of *Protogonyaulax tamarensis* and shellfish toxicity in the St. Lawrence Estuary:

689   freshwater runoff and the stability of the water column. p. 141-146. Anderson

690   DM, White AM, and Baden DG [eds.], Toxic Dinoflagellates. New York:

691   Elsevier.

692 Turner, J. T., and D. M. Anderson. 1983. Zooplankton grazing during dinoflagellate

693   blooms in a Cape Cod embayment, with observations of predation upon tintinnids

694   by copepods. Mar. Ecol. **4:** 359-374. doi:10.1111/j.1439-0485.1983.tb00119.x

695 Vardi, A., I. Berman-Frank, T. Rozenberg, O. Hadas, A. Kaplan, and A. Levine. 1999.

696   Programmed cell death of the dinoflagellate *Peridinium gatunense* is mediated by

697   CO_2 limitation and oxidative stress. Curr. Biol. **9:** 1061-1064. doi:10.1016/s0960-

698   9822(99)80459-x

699 Vardi, A. and others 2012. Host-virus dynamics and subcellular controls of cell fate in a

700   natural coccolithophore population. Proc. Natl. Acad. Sci. USA **109:** 19327-

701   19332. doi:10.1073/pnas.1208895109

702 Vardi, A. and others 2009. Viral glycosphingolipids induce lytic infection and cell death

703   in marine phytoplankton. Science **326:** 861-865. doi:10.1126/science.1177322

704 Velo-Suarez, L., M. L. Brosnahan, D. M. Anderson, and D. J. McGillicuddy. 2013. A

705   quantitative assessment of the role of the parasite *amoebophrya* in the termination

706   of *Alexandrium fundyense* blooms within a small coastal embayment. Plos One **8:**

707   e81150. doi:10.1371/journal.pone.0081150

708 Weise, A. M. and others 2002. The link between precipitation, river runoff, and blooms

709   of the toxic dinoflagellate *Alexandrium tamarense* in the St. Lawrence. Can. J.

710   Fish. Aquat. Sci. **59:** 464-473. doi:10.1139/f02-024

711

712 **Acknowledgements**

722

723 **Figure Legends**

724 **Fig. 1.** Map of Western Gulf of Maine showing the location of the study sites within the

725 Nauset Marsh System (NMS; inset). The locations of the two stations sampled for this

726 study are denoted by star symbols.

727

728   **Fig. 2.** Temporal (date) and spatial (depth) dynamics of the *A. fundyense* population at

729   Mill Pond (a) and Salt Pond (b) during 2013 bloom season, from March to May 2013.

730   The maximum mean concentration and the standard deviation of *A. fundyense* cells for

731   each sampling date shows cell abundance as logarithmic scale. In some cases, error bars

732   do not exceed the symbol width.

733

734   **Fig. 3.** Cell mortality in the *A. fundyense* population shown as percentage (mean ±

735   standard deviation) dead cells (left axis, black circles), ROS generation (left axis, white

736   circles) and caspase activity (left axis, grey circles) for associated cell death features in

737   Mill Pond (a) and Salt Pond (b). *A. fundyense* infection rates with *Amoebophrya* spp.

738   maturation stage (left axis, white circles for early stage, grey circles for intermediate

739   stage and black circles for mature stage) and *Amoebophrya* spp. dinospore dynamics

740   (right axis, black dotted line) in Salt Pond are shown in (c). Depth distribution of two loss

741   factors, cell death and infections with *Amoebophrya* spp., in the *A. fundyense* population

742   is shown as proportions of dead cells (mean ± standard error, left axis, white circles 1m,

743   grey circles 3m and black circles 5m) and infected cells (left axis, open diamonds 1m,

744   open triangles 3m and open squares 5m) from 1 m, 3 m and 5 m depths in Salt Pond (d).

745   *A. fundyense* cell densities as presented in Fig. 2 are shown here as interpolated lines

746   (right axis, black solid line) to visualize the impacts of loss factors over the bloom

747   progression.

748

749   **Fig. 4.** Total cell abundance (right axis, line) and the mean cell size (mean ± standard

750   error, left axis, open circles) of *A. fundyense* population over the bloom period in Salt

751   Pond, describing decreases in cell sizes until the peak of the bloom followed by increases

752   as the bloom declines (a). Estimated proportion of *A. fundyense* population as gametes

753   (black), vegetative cells (white) and planozygotes (grey) over the bloom progression in

754   Salt Pond based on the cell size analysis in this study (b).
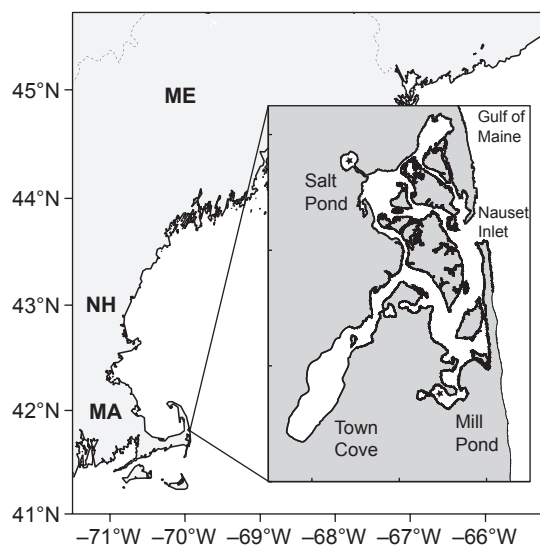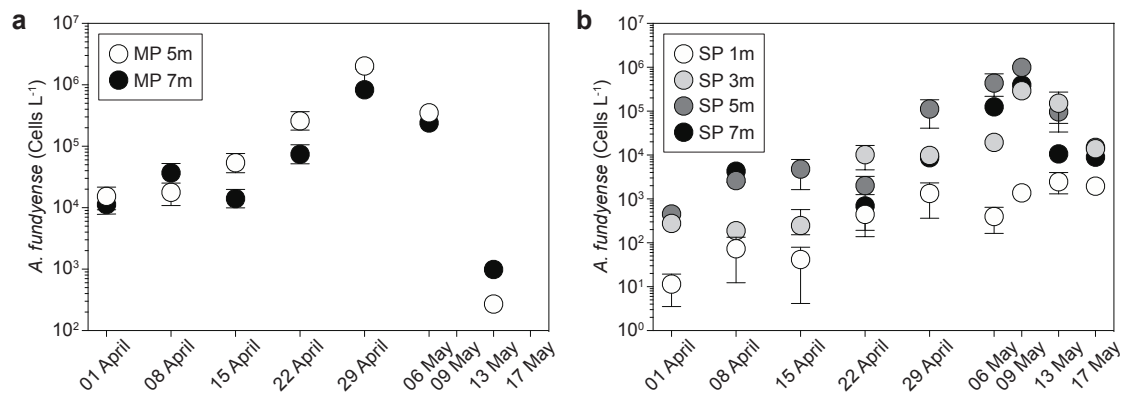
Fig. 1.

Fig. 2.

Fig. 3.

Fig. 4.

a — Mean cell sizes (μm³); A. fundyense (Cells L⁻¹)

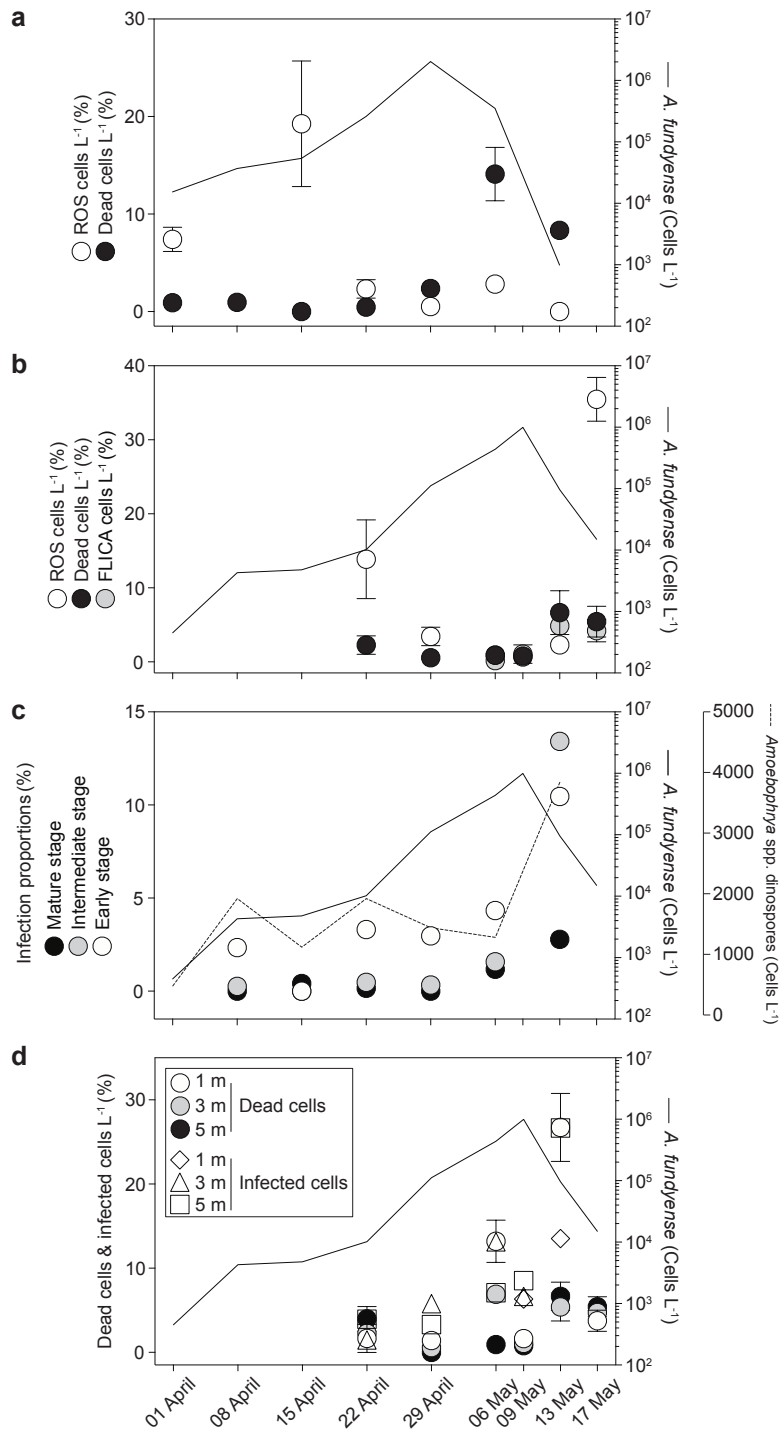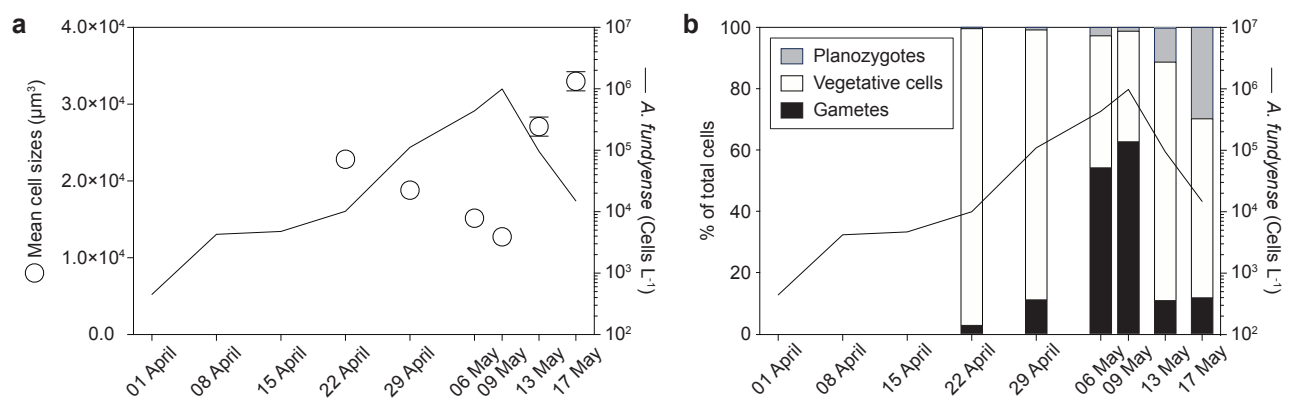**b** — Planozygotes; Vegetative cells; Gametes; % of total cells; A. fundyense (Cells L⁻¹)

1   **Supplemental Information**

2

3   **Insights into the loss factors of phytoplankton blooms: The role of cell mortality in**

4   **the decline of two inshore *Alexandrium* blooms**

5

6   Chang Jae Choi[1,3], Michael L. Brosnahan[2], Taylor R Sehein[2], Donald M. Anderson[2] and

7   Deana L. Erdner[*,1]

8

9   [*]Corresponding author: Deana L. Erdner, The University of Texas at Austin, Marine

10   Science Institute, Port Aransas, TX 78373 USA phone: +1 361 749 6719; fax: +1 361

11   749 6777; e-mail: derdner@utexas.edu

12

13   [1]The University of Texas at Austin, Marine Science Institute, Port Aransas, TX 78373

14   USA

15   [2]Biology Department, Woods Hole Oceanographic Institution, Woods Hole, MA 02543

16   USA

17   [3]Current address: Monterey Bay Aquarium Research Institute, 7700 Sandholdt Road,

18   Moss Landing, CA 95039 USA

19

20   Content of this file:

21   Tables S1, S2

22   Figure S1

23   **Table S1.** Descriptive statistics on *A. fundyense* cell size (μm^3) distributions over the bloom period at Salt Pond. The significance of

24   differences among all samples was analyzed by means of the Kolmogorov-Smirnov test.

	22 April	29 April	6 May	9 May	13 May	17 May
Number of cells examined	250	361	754	773	311	389
Minimum	11073.1	8317.71	3625.68	2649.15	6145.84	5708.47
25% Percentile	18700.6	15028.1	10046.7	6873.46	19320.2	20397.9
Median	22193.1	17631.3	12975.4	10652.8	27400.1	29597.1
75% Percentile	26626.8	21226.9	17498.1	16575.8	33206.1	42684.2
Maximum	67964.5	82973.7	87104.0	66517.4	67375.5	95345.3
Mean	22848.7	18824.3	15172.3	12744.1	27091.9	32987.4
S.D	5904.06	6350.19	8752.83	8030.2	10677.3	17477.3
S.E.M	373.405	334.221	318.759	288.826	605.452	886.135
P value	<0.0001	<0.0001	<0.0001	<0.0001	<0.0001	<0.0001

25

26

27

28

29

30

31

32   **Table S2.** Estimated daily contribution of cell loss processes to bloom decline from all depths.

	Cell abundance	% Infection (day^{-1})	Cell loss to infection (day^{-1})	% Daily loss contribution by infection	% Cumulative loss contribution by infection	% Cell death (day^{-1})	Cell loss to death (day^{-1})	% Daily loss contribution by cell death	% Cumulative loss contribution by cell death
9 May	422922[1]	2.79[1]	11783	7.05	7.05	2.10[1]	8861	5.30	5.30
10 May	255696[2]	5.09[2]	13025	13.63	9.44	8.73[2]	22313	23.35	11.86
11 May	160131[2]	7.40[2]	11852	19.80	11.36	15.36[2]	24593	41.09	17.28
12 May	100282[2]	9.71[2]	9737	23.35	12.73	21.99[2]	22051	52.88	21.36
13 May	58579[1]	12.02[1]	7039	36.57	13.93	28.62[1]	16766	87.10	24.66
14 May	39330[2]	12.98[2]	5106	34.74	14.70	24.07[2]	9466	64.40	26.12
15 May	24631[2]	13.95[2]	3436	37.32	15.21	19.51[2]	4807	52.21	26.71
16 May	15425[2]	14.92[2]	2301	42.53	15.57	14.96[2]	2308	42.66	26.92
17 May	10015[1]	15.88[2]	1591	40.12	15.80	10.41[1]	1043	26.29	26.92

33   [1] Observed value; [2] Calculated value

34

35

36

37

38

39

40   **Fig. S1.** Changes of the *A. fundyense* cell size distributions over the bloom period in Salt

41   Pond. The mean size of the cells during the early phase of the bloom (22 April) is

42   denoted by the vertical black lines as a baseline of the cell size. The mean cell size at

43   each sampling time is indicated by red lines. The overall shift in the mean cell sizes is

44   represented by the arrows.

Fig. S1.